X-621-75-6
PREPRINT

NASA TM X-70828

BEHAVIOR OF THE SODIUM AND HYDROXYL NIGHTTIME EMISSIONS DURING A STRATOSPHERIC WARMING

JEARL D. WALKER
EDITH I. REED

JANUARY 1975

GSFC
GODDARD SPACE FLIGHT CENTER
GREENBELT, MARYLAND

For information concerning availability
of this document contact:

Technical Information Division, Code 250
Goddard Space Flight Center
Greenbelt, Maryland 20771

(Telephone 301-982-4488)

Presented at the AMS Upper Atmosphere Meeting
Atlanta, Georgia, September 1974
Submitted to Journal of the Atmospheric Sciences

Behavior of the sodium and hydroxyl nighttime emissions during a stratospheric warming

Jearl D. Walker
Department of Physics
Cleveland State University
Cleveland, Ohio 44115

Edith I. Reed
Laboratory for Planetary Atmospheres
NASA/Goddard Space Flight Center
Greenbelt, Maryland 20711

Abstract

The behavior of the sodium and hydroxyl nighttime emissions during a stratospheric warminghas been studied principally by use of data from the airglow photometers on the Ogo-4 satellite. It was found that during the late stages of a major warming, both emissions increase appreciably, with the sodium emission returning to normal levels prior to the decrease in hydroxyl emission. The emission behaviors are attributed to temperature and density variations from 70 to 94 km, and a one-dimensional hydrostatic model for that altitude range is used to calculate the effects on the emissions and on the mesospheric ozone densities.

1. Introduction

During a major stratospheric warming the circulation in much of the winter hemisphere is altered and the temperature profile undergoes profound changes in both the stratosphere and lower mesosphere. There is some evidence that the upper mesosphere and lower thermosphere are also altered, as seen from considerations of measured and extrapolated temperature profiles (Labitzke, 1972 a, b; Mukherjee and Murty, 1972), from studies of the ionosphere (Entsian et al., 1971), and from observations of the sodium abundance (Hunten and Godson, 1967; Rundle and Sullivan, 1972) and hydroxyl airglow (Shefov, 1972). In this paper we shall examine variations in the sodium and hydroxyl night emissions as

measured by the Ogo-4 satellite during the major stratospheric warming in the winter of 1967-68. These emissions originate at altitudes near 90 km, and their variations can be interpreted in terms of atmospheric temperature and density variations in that altitude range. We will show these higher altitude variations are coupled with the 1967-68 stratospheric warming.

The airglow photometer (Reed et al., 1973) on the polar-orbiting satellite observed the nighttime emissions in the nadir direction in a number of wavelength regions (Table 1). Of interest here are the data for the (9-3) band of OH near 6230 A and for the 5890 and 5896 A lines of Na. The data for the 3914 A emission of N_2^+ were used to identify nonauroral conditions.

The OH emission is attributed to reaction (1) of Table 2, that is, to the reaction between ozone and atomic hydrogen. The most important loss mechanism appears to be a reaction with atomic oxygen (reaction (10)). The excited OH is the source of the extensive set of Meinel bands that dominate the red and near infra-red portions of the night airglow spectrum. From both rocket profiles and theoretical considerations, the emitting region is located between 75 and 100 km (see Table 3). Shefov (1972) has noted that during the 10 to 12 days after a stratospheric warming has appeared at the 25 km level, the intensity of the OH emissions increase by up to 50% with a 20 K increase in rotational temperature.

The sodium emission, as shown by various rocket profiles, occurs between 85 and 100 km (Table 4.). It has been explained by several different reaction schemes (see the review by Kvifte, 1973). The reactions used in this paper are reactions (2) through (9) of Table 2. Correlations between the sodium emission and stratospheric warmings have not previously been made. However, the abundance of sodium atoms near 90 km has been correlated with the temperature changes at 30 mb associated with stratospheric warmings (Rundle and Sullivan, 1972; Hunten and Godson 1967).

2. Stratospheric Warming of 1967-68

The stratospheric warming of 1967-8 was a major warming in the sense that it was accompanied by a complete circulation reversal. As summarized by Johnson (1969) and Labitzke (1968), it is seen that the warming at stratospheric levels first appeared in mid-December over Europe and moved rapidly north and west. Mesospheric temperatures above Scotland were much higher than normal (CIRA 1965) as early as December 13, and continued to increase reaching more than 70 K above CIRA data on December 21. During the first two weeks of January, the polar vortex was divided into cells; the winter circulation pattern was then gradually reestablished.

It was noted that the movement at the higher levels was much more rapid than at lower levels. By December 30 the warmest region at the 3-mb level had reached southwest Canada, while at the 10-mb

level, the main warm center was still coupled with the European anticyclone. In Pennsylvania a 50 to 60 K increase in mesospheric temperature on December 30 has been inferred from the anomalously high D-region radio absorption of that day (Rowe et al., 1969). Over Saskatoon, Canada, it was observed that the sodium layer near 90 km increased in abundance eleven days ahead of the increase in stratospheric (30-mb) temperatures (Rundle and Sullivan, 1972). Over Alaska the winds at meter levels (75-100 km) reversed just prior to and during the breakdown in the polar vortex (Hook, 1972).

Fig. 1 gives the synoptic maps (Staff, NOAA, 1971) January 10 in which meteorological data for January 7 to 13 is used. (Other weekly maps for December 1967 to January 1968 for 5 mb, 2 mb, and 0.4 mb can be found in Staff (ESSA, 1970) and Staff (NOAA, 1971) Johnson (1969).) The January 10 maps show the cold stratosphere centered near 75-80 N and 20 W at the altitudes of 51 km (0.4 mb) and 42 km (2 mb). At 35 km (5 mb) the cold center is near 55 N and 25 W (not shown here). By January 17 the cold centers at these three altitudes are close to the pole, with the normal hemispherical temperature distributions for winter being reestablished.

The rocket soundings over West Geirinish (57 N, 7 W), which is just south of the area analyzed in this paper, are available as temperature-time sections (Fig. 2) and are studied by Johnson (1969),

Labitzke (1972a), and Quiroz (1970, 1971). These sections indicate that between December 20 and 25 there is a substantial warming of the stratosphere from 40 to 50 km. Thereafter the warming layer appears to descend, and by January 3 the upper stratosphere from 30 to 55 km is isothermal and cold. The stratopause temperature peak is not evident again until January 10 to 11. There is evidently a warming near 65 km from January 6 to 10 that appears to be the lower edge of a mesospheric warming layer.

3. Photometer observations

A general inspection of the Ogo-4 photometer data for December 1967 and January 1968 showed that the data from the channels at 6225 A and 5890 A in the polar region were not symmetrical about the North Pole, but were much brighter at longitudes from 70 W to about 70 E than at Siberian longitudes. Figures 3a and 3b are examples of the January data for the Northern Hemisphere. A region including Greenland and Iceland, bounded by 60 N and 80 N latitudes and 0 and 50 W longitudes, was chosen for further study. The data for the OH and Na channel data in this region are shown in Figure 4.

From the spectrum of Broadfoot and Kendall (1968), it is apparent that both the OH (9-3) band and a continuum can make substantial contributions to the data from the channel at 6225 A. Fishkova (1969), however, noted that the continuum near 6220 A is seldom greater than 5 rayleighs/A. The contribution of manmade lights in the very thinly populated area under study is small. Hence, it is concluded that, in the absence of aurora, the major portion of the emissions observed by the channel at 6225 A is from the (9-3) band of OH.

The filter centered at the wavelengths of the sodium doublet is also of sufficient width to observed continuum sources and the (8-2) bands of OH. In this thinly populated area, however, the contribution made by sodium vapor lamps is negligible. The portion due to continuum and OH is assumed to bear a constant relation to the emissions observed in the 6225 A channel, with the result that in the region under study, 10 to 40% of the emission observed in the 5890 A channel is attributed to sodium. The sodium data presented here is the 5890 A channel data after subtraction of the continuum and OH emissions.

The observed data are in fact (1+a) times the column emission rate where a is the albedo of the earth and its atmosphere below the spacecraft. The value of a can range from less than 0.1 if the entire field of view is filled with clear, foam-free ocean to about 0.8 if the entire field of view is filled with a cloud deck. Since much of the area under study is ice or snow covered, with frequent fog and clouds, it is expected that the average albedo is on the order of 0.5. Since the albedo corresponding to each data point is not known, a specific correction cannot be made. However, it is to be noted that the observations in the 6225 A and 5890 A channels are made over practically identical areas; hence, changes in albedo would affect both equally.

Since aurora occurs frequently in this region, it was necessary to determine the extent to which auroral conditions contributed to the emissions in the channels at 6225 A and 5890 A. Several of the

N_2 First Positive bands appear in the passband of both channels (e.g., see Chamberlain, 1961, p. 184). The Na could be excited by electron-excited N_2 (Omholt, 1971); the [OH*] could be increased if mesospheric O_3 is increased by the presence of auroral particles (Maeda, 1968; Maeda and Aikin, 1968). Of particular interest are the substantial increases in Na and OH emissions observed on January 5-7.

To investigate these possible auroral effects, data for the three orbits on those days are plotted in Figure 5 along with the Ogo-4 data for the principal auroral lines at 3914 A, 5577 A and 6300 A. As is typical of aurora, there is a close correlation between the 3914 A and 5577 A lines; these come mainly from auroral particles which penetrate to below 150 km. The 6300 A emissions are characteristic of auroral energy deposited at levels above 200 km.

From an inspection of the curves in Figure 5, it is evident, particularly near 65 N for orbit 2365, that there is an increase in the observed emissions of OH and Na which is associated with aurora. The observed sodium emission is increased by about 20 R (rayleighs) per kR at 3914 A. The observed OH emission is increased by about 50 R/100 A per kR at 3914 A. It is evident that changes in auroral emissions cannot account for the decrease in the general level of the sodium emissions nor for the large increase in the OH emissions which appear in orbits 2394 and 2395 as compared to the values in orbit 2365.

The Ogo-4 data of Fig. 4 only extends from December 27 to January 8 and from January 24 to 28; data at other times in December and January were precluded by the presence of moonlight or sunlight. The daily averages for the OH and Na data for the region are given in Fig. 6a. The measurements in the analyzed region were made at a local time of 3:00 to 5:00 a.m. in December and early January and about 1:30 a.m. in late January.

Of particular interest is the general trend of the Ogo-4 data. Fig. 6a indicates that the Na values increase from late December to early January and are greatest on January 3, 4, and 5, but are noticeably lower on January 7 and 8. The values of the OH are also lower in December and increase with time, but are greatest on January 7, and then decrease. The changes in the OH values are readily apparent in Fig. 4b.

The daily 5 mb (35 km) and weekly 0.4 mb (51 km) temperatures for the center of the region of interest are given in Fig. 6b. The development of the stratospheric warming can first be seen at 0.4 mb and then later at 5 mb as the warming layer descends. It is after the 5 mb curve decreases that the Na and OH emissions begin to increase, both reaching peak emission rates when the 0.4 mb curve is near its lowest value. For the discussion to follow, it is important to note that the emissions are greatest when the upper stratosphere is cold and nearly isothermal.

Figs. 3a and 3b are polar maps of the OH and Na data for January 7. Data on these maps of interest to this paper are in Orbits 2394 and 2395, 60 N to 80 N, and can be located in Figs. 4a and 4b also.

Interpolation of the emission rates are made between orbits to facilitate drawing these maps. In Fig. 3a there is an area of high OH values centered near 0 W and 75 N. The corresponding Na values are relatively low, especially with respect to values 20 to 60 degrees to the east at the same latitude. Fig. 6b shows that by January 7 the stratosphere had undergone a large warming and the warming layer had descended. The 0.4 mb (51 km) temperature field (Fig. 1a) indicates an unusually cold region centered near 20 W and 75 N. Synoptic maps at 2 mb (42 km) (Fig. 1b) and 5 mb (34 km) (not shown here) for the same time indicate that not only is this region unusually cold, but also it is almost isothermal over the altitude range 34 to 51 km. The West Geirinish temperature measurements (Fig. 2) slightly to the south (57 N, 7 W) also show an isothermal upper stratosphere in early January. Such a cold, isothermal temperature profile for the upper stratosphere is one stage in a major stratospheric warming phenomenon. According to Labitzke (1972a, b), it is when such a stratospheric temperature profile occurs that the mesosphere should be experiencing a warming. The general geographical correlation of the cold, isothermal stratosphere region with the unusually large OH values suggests that a mesospheric warming may be responsible for the large increase in the OH nightglow emission.

Before attributing the changes in sodium emission to changes in the mesopheric temperature profile, it is proper to consider the possibility of an increase in free atomic sodium from such sources as meteors (Gadsden, 1971; Hake et al., 1972) and comet dust showers (Visconti and Fiocco, 1973). According to Hindley (1968), the peak

of the Quadrantid visible meteor shower (right ascension=232° and declination = 50° in 1950) occurred about noon GMT on January 4, 1968, and took about 19 hours to go from quarter maximum rate to quarter maximum rate. The enhanced sodium emission in the Ogo-4 data is first noticeable on January 3, orbit 2336 at 2:49 GMT, well ahead of the visible meteor shower; the emissions as measured from Ogo-4 appear to have no correlation with the visible shower. The radio meteor data available for this period is incomplete, but Gadsden has already shown that there is no apparent correlation between radio meteors and free sodium content. Finally, according to Poultney (1974), there were no comet dust showers during the Ogo-4 measurements analyzed here. Hence there is no evidence that these changes in the sodium emission rate can be attributed to changes in free sodium of extraterrestrial origin.

4. Mesospheric Warmings

Labitzke (1972 a, b) proposes that during a stratospheric warming, the mesosphere undergoes temperature variations that are out of phase with those in the upper stratosphere. Such a coupled behavior between the stratosphere and mesosphere should be most noticeable during a major stratospheric warming because of the larger temperature variations involved. As the 50 km region initially warms, the mesosphere would cool. Then as the stratospheric warming layer descends, leaving a cold 50 km region, the temperature at high levels would increase.

Data to support this theory comes primarily from rocket sondes and are generally available for altitudes less than 60 km. However, there are two series of measurements, one at Thumba, India (9 N, 77 E) and another at Pt. Barrow, Alaska (71 N, 157 W), that go to 80 km (Labitzke, 1972b). Mukherjee and Murty (1972) analyze the tropical measurements in detail and find significant stratospheric warming events. The mesospheric temperatures near 80 km are generally out of phase with those at 50 km. For example, a maximum warming of 37 K was seen at 55 km while a cooling of 44 K was seen at 80 km. A warm layer from 68 to 80 km was seen to increase by about 45 K within three weeks. Similar layers are used in our model to be discussed below.

5. Emission Chemistry

The examination of the observations indicates that the hydroxyl and sodium emissions increased at about the same time that increased temperatures would be expected in the upper part of the mesosphere. In this section we shall examine the effect that an increased temperature would have in terms of the reaction schemes which have been proposed for the sodium and hydroxyl reactions.

The OH emission is generally believed to be produced by the reaction between ozone and atomic hydrogen (reaction (1) of Table 2), releasing 3.34 eV and leaving the OH in the 8th or 9th vibrational level. The molecule then makes a radiative transition to lower vibrational levels, thereby producing the OH nightglow. Fiocco and Visconti

(1974) have found that the production rate of the 9th vibrational level is about 1.5 times that of the 8th level; we shall assume that this ratio remains constant with temperature. The radiative lifetime of the 9th level is 6.4×10^{-2}s (Potter et al., 1971). Loss by O_2 and N_2 quenching (reactions (15) and (16) of Table 2) is sufficiently small so as to be negligible in the upper part of the mesosphere. More important is the loss through reaction (10) with atomic oxygen.

Neither the source and layering of the free sodium nor the chemistry leading to the sodium nightglow are fully understood. A number of reaction schemes have been proposed, but the choice between them is not clear, partly because the rates of some of the proposed reactions are not well established and partly because the atmospheric number densities of some of the proposed reactants have not been measured. Hence, we will consider several of the schemes in our attempt to reproduce the observed airglow variations. Critical reviews of the sodium chemistry may be found in Donahue (1967), Srivastava and Shukla (1970), and Guenther (1974).

Early consideration of the number of free sodium atoms (as observed from twilight glow) and the number of photons emitted during the course of the night indicated that the series of reactions leading to the nightglow must not result in an appreciable net change in the number density of the free sodium atoms. The first such set of reactions was proposed by Chapman (1939), reactions (2), (3), and (4) of Table 2, which involve oxidation of Na by O_3 followed by reduction by O.

However, the reaction rates are not certain and may not be sufficiently high to account for the airglow. Bates and Nicolet (1950) have proposed a scheme involving O_2, H, and O, reactions (6), (7), and (8) of Table 2. Bates (1954) modified this scheme using H instead of O, reaction (9). Donahue (1967) has proposed that the Na is excited by vibrationally excited O_2, reaction (5), the O_2* being produced as the result of reactions (11) and (12), and balanced in part by the loss of O_2* through equation (13).

Since current knowledge does not permit a certain choice from among these schemes, each will be used in our attempt to reproduce the behavior of the sodium nightglow during a stratospheric warming. It must be noted, however, that proper treatment of the problem necessitates that the temperature dependence of each reaction rate be explicitly known, but these dependences are in fact not known for several of the reactions.

6. Emission rates

If the mesopheric density and temperature vary, there should be accompanying variations in the mesospheric nightglows, both because the nightglows are sensitive to density variations since they are due to two or three body reactions, and because the reaction rates of some of the relevant reactions are temperature dependent.

The emission rates J (photons sec^{-1} cm^{-3}) for the OH (9-3) band and the sodium lines are expressed as

$$J(OH) = [OH^*]A_1 \qquad (1)$$

$$J(Na) = [Na^*]A_2 \qquad (2)$$

where A_1 = 15.63 s^{-1}, which is the sum of the transition probablilities from the ninth vibrational level to lower vibrational levels of OH, that is, the inverse of the radiative lifetime of the ninth level. A_2 is the mean transition probability, 6.29 x 10^7 s^{-1}, for the Na D-line transitions.

To find an expression for steady state [OH*] from reaction (1), the steady state of [O_3] is calculated assuming that reaction (14) is the principal mechanism for production and that reactions (1) and (12) are the primary loss mechanisms. Since the Ogo-4 observations analyzed here are all from well after midnight, it can be assumed that the nighttime steady state conditions for [O_3] have been attained (Dütsch, 1971). The steady state density of O_3 is then given by

$$[O_3] = (k_{14}\,[O]\,[O_2]\,[M]) \;/\; (k_1\,[H] + k_{12}\,[O]) \quad . \qquad (3)$$

Taking into account the loss of OH* (v= 9) through equation (10), the emission rate of OH (9-3) can be written as

$$J(OH) = \frac{A_1\,k_1\,k_{14}\,[O]\,[O_2]\,[M]\,[H]}{(A_1 + Q_1)\,(K_1\,[H] + k_{12}\,[O_2])} \quad , \qquad (4)$$

where $Q_1 = 10^{-10}\,[O]\ s^{-1}$.

A similar calculation is performed for the sodium emission. Using the Chapman sodium nightglow mechanism, reactions (2) through (4), quenching by the molecular constituents as in reactions (17) and (18), and the steady state density of O_3 as given by equation (3), the emission rate may be expressed as

$$J_c(Na) = \frac{A_2\, k_2\, k_{14}\, [O]\, [Na]\, [O_2]\, [M]}{(A_2 + Q_2)\, (k_1[H] + k_{12}[O])} \quad , \qquad (5)$$

where $Q_2 = k_{17}\, [N_2] + k_{18}\, [O_2]$.

For the O_2^* mechanism for the excitation of sodium, reaction (5) of Table 2, the density of O_2^* is computed from reactions (11), (12), and (13) as follows:

$$[O_2^*] = (k_{11}\, [O]\, [M] + k_{12}\, [O_3])/k_{13} \quad . \qquad (6)$$

Using this, $[O_3]$ as given by equation (3), and Q_2 as defined above, the sodium emission from O_2^* excitation may be expressed by

$$J_{ox}(Na) = \frac{A_2\, k_5\, [Na]\, [O]\, [M]}{k_{13}\, (A_2 + Q_2)} \left(K_{11} + \frac{k_{12}\, k_{14}\, [O_2]}{k_1\, [H] + k_{12}\, [O]} \right) \quad . \qquad (7$$

The Bates and Nicolet (6-8) and Bates (6, 7, 9) proposals lead to

$$J_B\, (Na) = A_2\, k_6\, [Na]\, [O_2]\, [M]\ \ (A_2 + Q_2\ )^{-1} \quad . \qquad (8)$$

In our calculations [M] is taken to be the atmospheric density as given by U.S. Standard Atmosphere Supplements (1966). The $[O_2]$ and [H] values are estimated from Hunt (1973). The relative insensitivity of our results to the $[N_2]$, $[O_2]$, and [H] values is considered below. We represent the [O] values by the expression (Reed and Chandra, 1974):

$$[O] = [O]_m \exp 1/2\ (1 - \frac{(z - z_m)}{Sh} - \exp \frac{-(z - z_m)}{Sh}) \quad , \qquad (9)$$

where [O] is the oxygen density at the altitude z, z_m is the altitude of the maximum oxygen density $[O]_m$, h is the scale height of a mixed

atmosphere, and S is a parameter dependent upon the degree of mixing. We use $[O]_m = 1.48 \times 10^{12} cm^{-3}$, $z_m = 95.2$ km, $h = 5.41$ km, and $S = 0.69$. The computed [O] is within a few percent of the Jacchia (1971) model values from 90 to 100 km. Lower values of [O] are found in other models, for example, Hunt (1973), but their use would alter our results (Table 5, to be discussed below) by less than a few percent.

The normal, prewarming OH and Na emission profiles are taken to be vertical Gaussian functions, with altitude widths at half-maximum emission rate of 8 km for OH and 4 km for Na. The peak density of atomic Na is taken to be at 90 km, which is consistent with the winter observations of Sullivan (1971) at Victoria, British Columbia. Both Sullivan's data and the Ogo-4 data are for Na at high latitudes in the Northern Hemisphere for midwinter. Both the altitude of peak density and the vertical distribution with full width at half-maximum density of 4 km are consistent with the Gibson and Sanford (1971) laser observations of the winter Na layer at 51 N, 1 W. For the OH emission, the peak emission altitude of 85 km and the vertical width of 8 km are consistent with observations of Rogers et al. (1973) and Packer (1961) and theoretical calculations of Fiocco and Visconti (1974) and Gattinger (1971).

The columnar emission rates for the OH and Na nightglows, such as is measured by the Ogo-4 photometer, are found by integrating (4), (5), (7), and (8) over the emitting layers.

7. Mesospheric Warming Model

OH and Na nightglow variations similar to those of the Ogo-4 observations are modeled with temperature and density variations that are consistent with the Labitzke (1972a, b) predictions of a mesospheric temperature change during a major stratospheric warming. When the stratosphere near 50 km warms during the initial stage of a stratospheric warming, the mesosphere, according to Labitzke, cools. As the stratospheric warming layer then descends, resulting in a relatively cool and nearly isothermal region near 50 km, the mesosphere warms.

The mesospheric temperature variations and the accompanying density changes should cause variations in the OH and Na nightglow emission rates. Here we simulate such nightglow variations during the predicted warming of the mesosphere by superimposing a warm layer on a "standard atmosphere" model of the mesosphere. The standard temperatures and densities are calculated by taking the temperature and density at 60 km to be those given in the U. S. Standard Atmosphere Supplements (1966) for January at 60 N, and then using the following hydrostatic equation to find the temperatures and densities at higher altitudes. The atmospheric density $\rho(z)$ at height z km above a chosen base is

$$\rho(z) = \rho_0 \, (T(z)/T_o)^{-(g/R\alpha + 1)} \quad , \qquad (10)$$

(Quiroz, 1970) where ρ_0 and T_0 are the density and temperature at the base, T(z) is the temperature at a height z km above the base, g is the gravitational acceleration, and R is the gas constant for dry air. The lapse rate α is taken as positive when there is an increase in

temperature with altitude. A lapse rate of -2.152 deg-km^{-1} is used up to a mesopause at 90 km, above which the lapse rate of 1.617 deg-km^{-1} is used. The resulting temperatures (Fig. 7a, "standard profile") are generally within 0.5 K and the resulting densities within a few percent of those values given in the 1966 Supplements for the altitude range of 60 to 95 km.

In our scheme to explain the Ogo-4 nightglow variations of Fig. 6(a), the mesospheric warming layer first develops near 80 km (Fig. 7a) and then descends and expands downward while 80 to 90 km cools and above 90 km warms (Fig. 8a). The triangular temperature profiles are similar to those used by Quiroz (1970, 1971) for stratospheric warmings. The altitude ranges experiencing the temperature changes are chosen primarily to produce calculated nightglow variations similar to those of Fig. 6(a). Other profiles of temperature changes with different shapes and greater ranges of altitude could be devised to yield approximately the same results. In particular, it may be desirable to choose a broader warming layer so that the maximum change in temperature from standard values need not be as large as we use (Figs. 7b and 8b). The temperature changes employed in our model are similar to those reported by Mukherjee and Murty (1972) for a tropical warming.

The associated density variations (Figs. 7b and 8b) are calculated by (10). Quiroz (1970) makes such calculations for stratospheric density changes during a stratospheric warming. In both density and temperature, we attempted to minimize the variations above 95 km.

The variations in the OH and Na emission rates due to the warming layer in our model are calculated by (4), (5), (7), and (8) and are shown in Figs. 7c, 7d, 8c, and 8d as functions of altitude. Integrations over the emission layers give the variations in columnar emission rate as a ground or satellite observer would measure them and which can be compared to the Ogo-4 measurements. However, rather than duplicating the Ogo-4 OH and Na data with our mesospheric warming layer, we limit our present analysis to simulating the general trend of the variations of the measured nightglows during the stratospheric warming.

8. Calculated nightglow changes

Computations of the changes in the OH and Na columnar emission rates in going from prewarming conditions (denoted PW) to the temperature profiles of Figs. 7 and 8 (denoted by figure number) are summarized in Table 5. The Chapman mechanism (2,3,4) is denoted by C; the O_2* mechanism (5) is denoted by Ox; and the Bates and Nicolet mechanisms (6-9) are denoted by B. As the mesospheric warming first develops into the Fig. 7a profile, the OH emission brightens slightly and the several Na emission schemes all give a brightening of the Na emission. When the mesospheric warming changes from the Fig. 7a profile to the Fig. 8a profile, the OH emission brightens more, as does the Na emission when the O_2* scheme is considered. The Bates and Nicolet schemes give no change in the Na emission. The Chapman scheme, however, leads to a decrease in the Na emission that leaves the emission at only 42% of its prewarming value. The Chapman scheme results in the decrease for Fig. 8 conditions in spite of the above

normal densities in the Na layer, as seen in Fig. 8b at 90 km, because the Chapman scheme is very dependent on the $[O_3]$ which is low at 90 km (Fig. 8e) due to the temperature dependence of k_{14}. The O_2^* mechanism is also dependent on $[O_3]$ but to a lesser extent, and the mechanism yields an increase in Na emission because of the overall atmospheric density increase near 90 km (Fig. 8b) and the temperature dependence of k_{12}. The temperature dependence of the reaction rates k_6, k_7, k_8, and k_9 employed in the Bates and Nicolet schemes are not known and hence, those schemes reflect only the increase in atmospheric density from the prewarming values. Since the overall density increase at 90 km is about the same for both Fig. 7 and Fig. 8 situations, the Bates and Nicolet schemes do not result in an emission change in going from the conditions of one figure to the other. If the temperature dependences of the reaction rates were known and included in the calculations, this result could, of course, be different.

In our calculations we assume that $[O_2]$, $[N_2]$, [O], and [H] vary directly with the overall atmospheric density variations. With that assumption, the results of Table 5 are not very sensitive to the initial vertical profiles or the absolute values of those constituents. Halving or doubling the absolute values alters the table's results by less than a few percent.

We also assume that [Na] varies directly with the atmospheric density. Blamont and Donahue (1964) give the free Na density as a function of the total Na in both free and combined forms. Since the hydrogen reactions may be ignored, the form of the equation is as given by Guenther (1971)

$$Na = \frac{Na + NaO + NaO_2}{1 + 2.64 \times 10^{-22} [O_2] \frac{[N_2]}{[O]} + 0.16 \frac{[O_3]}{[O]}} \qquad (11)$$

We have incorporated into (11) the appropriate reaction rates as reported by Srivastava and Shukla (1970). If we use density values of $[O_2]$, $[N_2]$, and $[O]$ as discussed above, and our computed values of $[O_3]$, we find that nearly 100% of the Na is in free form at 90 km. Hence, the total Na abundance in the Na layer may remain constant during the mesospheric warming unless there is vertical transport of free Na or Na compounds into the layer. The above expression for [Na] may not be complete, however, and in particular does not include Na ion chemistry (Swider, 1969, 1970). If the free Na abundance does remain constant, the computed variations in the Na emission are altered. These altered values are given in Table 5 on the second lines for each of the three types of ratios and for each of the Na emission mechanisms.

According to the Labitzke predictions (1972a, b) and the Mukherjee and Murty observations (1972), the mesospheric warming develops after the stratosphere near 40 and 50 km has passed its peak temperature and has begun to cool. Fig. 6 gives the Na and OH channel data and the temperatures near 51 and 35 km in the region of interest. The Na and OH emission rates appear to be on the proposed schedule. When the 35 km temperatures begin to

decrease, the emission rates begin to increase, implying that the mesospheric warming layer begins to develop. The high altitude (near 65 km) warming for January 6-8 in the West Geirinish temperature-time section of Fig. 2 can be interpreted as the lower edge of the mesospheric warming layer of the model depicted in Fig. 8a.

The overall trend of our modeled emission changes is similar to that of the Ogo-4 observations in late December and early January discussed above and shown in Fig. 6a. If we identify the prewarming conditions in the mesosphere with December 30, the Fig. 7 conditions with January 4, and the Fig. 8 conditions with January 7, then Table 5 summarizes both the computed and observed emission variations. The observation numbers are calculated from Fig. 6a.

There is satisfactory agreement between the model calculations and the observations for the OH emission, especially in the change from Fig. 7 conditions to Fig. 8 conditions. To find a closer fit with the OH results, there would have to be a greater increase in $[O_3]$ in the OH emission layer for the situations corresponding to Figs. 7 and 8. In the case of Fig. 8, this may be simulated by having the cool layer presently at 85 km to extend to lower altitudes.

The Na emission does change with the introduction of a mesospheric warming. In our attempts to simulate in a general

way the Ogo-4 observations, we find the best agreement between observations and computations when using the Chapman mechanism because with that mechanism we obtain a Na emission decrease with the Fig. 8 conditions. We therefore simulate the nightglow variations of Fig. 6a in which both OH and Na emissions initially increase and then the Na emission decreases as the OH emission continues to increase. With our Fig. 7 and 8 temperature models, the O_2^* mechanism continues to increase the Na emission as the OH emission increases whereas the Bates and Nicolet mechanisms do not alter the Na emission as the OH emission increases. In order to decrease the Na emission with the O_2^* or the Bates and Nicolet mechanisms between Fig. 7 and Fig. 8, there would have to be a much steeper lapse rate and higher temperatures between 85 and 95 km in Fig. 8a.

Our results may also be consistent with Shefov's report (1972) of a 40 to 50% increase in the OH intensity 10 to 12 days after a stratospheric warming was detected at 25 km. Accompanying that OH increase was an apparent 15 K to 20 K increase in rotational temperature. This may mean a 15 K to 20 K increase in ambient temperature at the OH emission altitude. It is difficult to relate these numbers to our model calculation because density variations have not been accounted for in Shefov's report, and he does not relate more such observations nor the details of this one. Nevertheless, the OH intensity variation is similar to that studied here, although delayed by a few days from the time that the stratospheric warming

reaches the lower atmosphere.

The present calculations are based on several assumptions about

(1) the relevant nightglow reactions and reaction rates, including the quenching terms,

(2) the simple changes in atmospheric constituent densities proportional to the overall density changes (we have considered O_3 and Na as exceptions),

(3) the hydrostatic equilibrium conditions and the absence of horizontal and vertical transport,

(4) the initial Gaussian emission profiles with certain vertical widths and altitudes of peak emission, and

(5) the triangular shapes of the mesospheric warming layers,

among other factors. A real atmosphere with real emissions and warmings is certain to be much more complicated. Within these assumptions, however, there is general consistency of the Ogo-4 measurements with our model calculations (especially when using the Chapman mechanism for the Na emission) and hence, with the Labitzke predictions (1972a, b) of a mesospheric warming.

9. Mesospheric Ozone Changes

Independent evidence for a mesospheric warming is suggested by the data of Evans and Llewellyn (1972). The profile of mesospheric ozone can be inferred from measurements

of the O_2 emission at 1.27 μ. Evans and Llewellyn made ground based measurements of this emission and compared then to direct rocket measurements made by Vallance Jones et al. (unpublished) data, 1972). Some of the data were taken during a major stratospheric warming in January 1971. The ground-based measurements on January 16, 1971, at Ft. Churchill, Canada, showed a large decrease in the 1.27 μ emission rate from normal winter values, and this decrease implied a large decrease in the ozone above 80 km. The rocket measurements made on January 13, 1971, also showed the decrease in the emission rate.

Hilsenrath (1971) measured an increase by a factor of 4 in ozone density at 55 km in another winter, and he associates the increase with a 50 K decrease in the temperature at that altitude. The ozone chemistry at that altitude is somewhat different than we are presently considering for the upper mesosphere, but the associated temperature and ozone variations suggest that the Evans and Llewellyn results could be explained by a temperature increase in the mesosphere.

Labitzke (1972a) analyzed the Northern Hemisphere temperature fields for this 1971 warming using data from the Satellite Infrared Spectrometer (SIRS) on board Nimbus 4 and data from Selective Chopper Radiometer (SCR). The Stratospheric warming layer descended somewhat between January 6

and 13, 1971, but was still in the upper stratosphere. If this warming was similar to that of 1967-1968 discussed above, then there should have been a warming layer developing near the mesopause on January 13-16, 1971. Such a warming layer from 80 to 90 km would decrease the atmospheric density and the ozone density within the layer. Indeed, that smaller ozone density is seen in both the Vallance Jones data and the Evans and Llewellyn data. At 85 km they measured the ozone density as being about half the normal winter density at that altitude. If we assume a triangular warming layer similar to Fig. 7a, but from 80 to 90 km, we find from (17) that we need only a 25 K increase in temperature at 80 km to account for such a ozone decrease, a temperature variation within the range we consider above. Figs. 7e and 8e indicate the computed percentage changes in ozone density that we associate with our mesospheric warming model.

10. Summary

We have analyzed the OH and Na nightglow emission rates measured by Ogo-4 concurrently with the major stratospheric warming of December 1967 and January 1968. Both emissions increased from late December to early January, but then as the Na emission decreased, the OH emission continued to increase to an unusually high emission rate.

A one-dimensional hydrostatic model of the mesospheric temperature and density has been used to simulate the nightglow variations. We assumed the hydrogen and ozone reaction to be responsible for the OH emission and considered the Na excitation mechanisms of Chapman, Bates and Nicolet, and an O_2^* reaction. With appropriate choices of the mesospheric temperature profiles, the nightglows can be made to simulate the Ogo-4 results, especially when using the Chapman mechanism for the Na emission. In thus simulating the Ogo-4 results, there appears to be a mesospheric warming that occurs over the region of the stratospheric warming phenomenon. The model appears to confirm predictions that the temperatures of the mesosphere varies out of phase with the temperatures of the upper stratosphere during a major stratospheric warming event. Thus, the phenomenon we call a major stratospheric warming extends to at least the lower thermosphere near 100 km.

Acknowledgements: We would like to thank R. S. Quiroz and S. K. Poultney for many helpful comments in the preparation of this paper. Prof. Jacques E. Blamont of the Centre National de la Recherche Scientifique (France) was co-experimenter for the Ogo-4 Airglow Photometer Experiment.

Table 1. Ogo-4 filters and light sources seen through each.

Nominal Wavelength, A	Emissions and other light sources
3914	N_2^+ ($B^2\Sigma_u^+$) First Negative, aurora
	Unidentified band (Broadfoot and Kendall, 1968)
	Hg-vapor street lamps
	O_2 ($A^3\Sigma_u^+$) Herzberg bands, airglow
5577	O(^{1}S) airglow and aurora
	OH (7-1) Meinel airglow
	Continuum airglow
	Incandescent street lamps
5893	Na (^{2}P) airglow
	OH (8-2) Meinel airglow
	N_2 ($B^3\pi_g$) First Positive, aurora
	Continuum airglow
	Incandescent and Na-vapor street lamps
6225	OH (9-3) Meinel airglow
	Continuum airglow
	Incandescent street lamps
6300	O (^{1}D) airglow and aurora
	OH (9-3) Meinel airglow
	Continuum airglow
	Incandescent street lamps

Table 2. Chemical reactions

Reaction	Rate	Reference
OH emission:		
(1) $O_3 + H \rightarrow OH^* (v \leq 9) + O_2$	$k_1 = 1.5 \times 10^{-12} (T)^{1/2} cm^3 s^{-1}$	(Nicolet, 1971)
Chapman (1939) Na emission:		
(2) $Na + O_3 \rightarrow NaO + O_2$	$k_2 = 6.5 \times 10^{-12}$ cm^3 s^{-1}	(Srivastava and Shukla, 1970)
(3) $NaO + O \rightarrow Na^* (^2P) + O_2$	$k_3 = 4 \times 10^{-11}$ cm^{3}s^{-3} ^{1}	(")
(4) $Na^* (^2P) \rightarrow Na (^2S) + h\nu$		
O_2 reaction for Na emission (Donahue, 1967):		
(5) $Na + O_2^* \rightarrow Na^* (^2P) + O_2$	$k_5 = 3 \times 10^{-10}$ cm^{3}s^{-1}	
Followed by (4)		
Bates and Nicolet (1950) Na emission:		
(6) $Na + O_2 + M \rightarrow NaO_2 + M$	$k_6 = 2 \times 10^{-33}$ cm^{6}s^{-1}	(Srivastava and Shukla, 1970)
(7) $NaO_2 + H \rightarrow NaH + O_2$	$k_7 = 2.98 \times 10^{-12}$ cm^{3}s^{-1}	(")
(8) $NaH + O \rightarrow Na^* (^2P) + OH$	$k_8 = 1.71 \times 10^{-18}$ cm^{3}s^{-1}	(")
Followed by (4)		
Bates (1954) Na emission:		
Reactions (6) and (7), followed by		
(9) $NaH + H \rightarrow Na^* (^2P) + H_2$	$k_9 = 4.33 \times 10^{-17}$ cm^{3}s^{-1}	(Srivastava and Shukla, 1970)
Followed by (4)		
Other reactions used in this paper:		
(10) $OH^* + O \rightarrow O_2 + H$	$k_{10} = 5 \times 10^{-11} (1 + 0.11\ v)$ cm^{3}s^{-1} v = vibrational level	(Rogers et al., 1973)
(11) $O + O + M \rightarrow O_2^* + M$	$k_{11} = 3 \times 10^{-33} (300/T)^3$ cm^{3}s^{-1}	(Nicolet, 1971)
(12) $O + O_3 \rightarrow O_2^* + O_2$	$k_{12} = 2.4 \times 10^{-11} \exp(-2350/T)$ cm^{3}s^{-1}	(Nicolet, 1971
(13) $O + O_2^* (v) \rightarrow O_2^* (v' < v) + O$	$k_{13} = 10^{-10}$ cm^{3}s^{-1}	(Donahue, 1967)

(14) $O + O_2 + M \rightarrow O_3 + M$, $k_{14} = 3.3 \times 10^{-35} \exp(950/T)$ $cm^3 s^{-1}$ (Nicolet, 1971)

Quenching of OH*

(15) by N_2 $k_{15} = 1.0 \times 10^{-14}$ $cm^3 s^{-1}$ (Worley et al., 1972)

(16) by O_2 $k_{16} = 3.6 \times 10^{-15}$ $cm^3 s^{-1}$ (")

Quenching of Na*

(17) by N_2 $k_{17} = 1.88 \times 10^{-7}$ $cm^3 s^{-1}$ (Srivastava and Shukla, 1970)

(18) by O_2 $k_{18} = 3.80 \times 10^{-10}$ $cm^3 s^{-1}$ (")

Date	Local Civil Time	Latitude	Wavelength	Altitude	Reference
Nov. 6, 1959	0025	32°N	7220 - 7370 A 7400 - 1020 A	83 km 90	Packer, 1961
Sept. 23, 1960	night	mid	9100 - 10700 A	78, 88	Tarasova, 1966
Mar. 21, 1963	night	58	rot. temp	80 - 90	Noxon, 1964
April 28, 1966	2049	32	7210 - 7450	97	Baker and Waddoups, 1967
Jan. - Mar. 1968	night	high	6800 - 7100	85-100	Sivjee et al., 1972
Oct. 26, 1969	0040	75	8300 - 8460	95	Harrison, 1970
Mar. 6, 1972	0200	70	1.40-1.65 μm 1.85-2.12 μm	84	Rogers et al., 1973
Theoretical				82	Gattinger, 1971
Theoretical				84	Fiocco and Visconti, 1974

Table 3. Altitude of the peak emission rate for the hydroxyl emissions.

Date	Latitude	Altitude
Dec., 1955	41 N	84 km
July, 1956	"	93
March, 1957	"	89
Oct., 1961	28 N	93.5
Sept., 1960	mid-lat. N	82.5
Oct., 1965	41 S	89

Table 4. Altitude of the peak emission rate for the sodium emission, adapted from Greer and Best (1967).

Table 5. Emission-rate ratios

Ratios of columnar emission rates	Model results				Ogo-4 measurements	
	OH	Na			OH	Na
		C	Ox	B		
(Fig. 7)/ PW	1.02	1.32	1.27	1.27	1.41	1.19
		1.22	1.17	1.17		
(Fig. 8)/ PW	1.63	0.55	1.46	1.27	2.04	0.56
		0.50	1.35	1.17		
(Fig. 8)/(Fig. 7)	1.60	0.42	1.15	1.0	1.46	0.46
		0.41	1.15	1.0		

PW pertains to prewarming conditions.

(Fig. 7) and (Fig. 8) pertain to the temperature profiles given in those figures.

The second numbers in the model Na results are for a constant Na abundance.

The Ogo-4 data are the average values of Fig. 6a and we identify Dec. 30 as the prewarming conditions, Jan. 4 as Fig. 7, and Jan. 7 as Fig. 8.

References

Baker, D. J., and R. O. Waddoups, 1967: Rocket measurement of mid-latitude night airglow emissions, J. Geophys. Res., 72, 4881-4883.

Bates, D. R., 1954: The physics of the upper atmosphere, The Earth as a Planet, G. P. Kuiper, ed., Univ. Chicago, Chicago 576-643.

_____, and M. Nicolet, 1950: The photochemistry of atmospheric water vapor, J. Geophys. Res., 55, 301-327.

Blamont, J. E., and T. M. Donahue, 1964: Sodium dayglow: Observation and interpretation of a large diurnal variation, J. Geophys. Res. 69, 4093-4127.

Broadfoot, A. L., and K. R. Kendall, 1968: The airglow spectrum, 3100-10,000 A., J. Geophys. Res., 73, 426-428.

Chamberlain, J. W., 1961: Physics of the Aurora and Airglow, Academic Press, New York.

Chapman, S., 1939: Notes on atmospheric sodium. Astrophys. J., 90, 309-316.

Donahue, T. M., 1967: Sodium airglow. International Dictionary of Geophysics, S. K. Runcorn, ed., New York, Pergamon Press, 1417-1426.

Dütsch, H. U., 1971: Photochemistry of atmospheric ozone. Advances in Geophysics, Vol. 15, H. E. Landsberg and J. Van Mieghem, eds., New York, Academic Press, 219-322.

Entsian, G., S. S. Gaygerov, and D. A. Tarasenko, 1971: Midwinter warmings of the stratosphere and mesosphere and processes in the ionosphere. Izv., Atmos. Oceanic Phys., 7, 932-938.

Evans, W. F. J., and E. J. Llewellyn, 1972: Measurements of mesospheric ozone from observations of the 1.27 μ band. Radio Sci., 7, 45-50.

Fiocco, G., and G. Visconti, 1973: On the seasonal variation of upper atmospheric sodium. J. Atmos. Terr. Phys., 35, 165-171.

_____, and _____, 1974: Simultaneous measurements of the OH* nightglow in the (9-4), (8-3), and (5-1) bands and effects of quenching. J. Atmos. Terr. Phys., 36, 583-590.

Fishkova, L. M., 1969: Intensity distribution in the continuous airglow spectrum in the range λ 5500-6700A. Geomagnetism and Aeronomy, 9, 463-464.

Gadsden, M., 1971: Comparison of radio-meteor rate with abundance of sodium in the upper atmosphere. Ann. Geophys., 27, 401-406.

Gattinger, R. L., 1971: Interpretation of airglow in terms of excitation mechanisms. D region nightglow. The Radiating Atmosphere, B. M. McCormac, ed., Dordrecht-Holland, D. Reidel Publ. Co., 51-63.

Gibson, A. J., and M. C. W. Sandford, 1971: The seasonal variation of the night-time sodium layer. J. Atmos. Terr. Phys., 33, 1675-1684.

Greer, R. G. H., and G. T. Best, 1967: A rocket-borne photometric investigation of the oxygen lines at 5577 A and 6300 A, the sodium D-lines and the continuum at 5300 A in the night airglow. Planet. Space Sci., 15, 1857-1881.

Guenther, B. W., 1974: Observations from the Orbiting Geophysical Observatory VI of mesospheric airglow and scattering layers. Ph.D. Dissertation, Univ. Pittsburgh, Pittsburgh, Penn.

Hake, R. D., Jr., D. E. Arnold, D. W. Jackson, W. E. Evans, B. P. Ficklin, and R. A. Long, 1972: Dye-laser observations of the nighttime atomic sodium layer. J. Geophys. Res., 77, 6839-6848.

Harrison, A. W., 1970: Altitude profile of airglow hydroxyl emission. Can. J. Phys., 48, 2231-2234.

Hilsenrath, E., 1971: Ozone measurements in the mesosphere and stratosphere during two significant geophysical events. J. Atmos. Sci., 28, 295-297.

Hindley, K. B,. 1968: Meteor notes--January to June 1968. J. Brit. Astr. Ass., 79, 68-69.

Hook, J. L., 1972: Wind patterns at meteor altitudes (75-105 kilometers) above College, Alaska, associated with midwinter stratospheric warmings. J. Geophys. Res. , 77, 3856-3868.

Hunt, B. G., 1973: A generalized aeronomic model of the mesosphere and lower thermosphere including ionospheric processes. J. Atmos. Terr. Phys., 35, 1755-1798.

Hunten, D. M., and W. L. Godson, 1967: Upper-atmospheric sodium and stratospheric warmings at high latitudes. J. Atmos. Sci., 24, 80-87.

Jacchia, L. G., 1971: Revised static models of the thermosphere and exosphere with empirical temperature profiles. Smithsonian Astrophysical Observatory Special Report 332, Cambridge, Mass.

Johnson, K. W., 1969: A preliminary study of the stratospheric warming of December 1967-January 1968. Mon. Wea. Rev., 97, 553-564.

Kvifte, G. , 1973: Alkali chemistry problems of the upper atmosphere. Physics and Chemistry of Upper Atmospheres, B. M. McCormac, ed., Dordrecht-Holland, D. Reidel Publ. Co., 158-168.

Labitzke, K., 1968: Midwinter warmings in the stratosphere and lower mesosphere. Z. Geophys., 34, 555-561.

_____, 1972a: Temperature changes in the mesosphere and stratosphere connected with circulation changes in winter. J. Atmos. Sci., 29, 756-766.

_____,1972b: The interaction between stratosphere and mesosphere in winter. J. Atmos. Sci., 29, 1395-1399.

Maeda, K., 1968: The auroral O_2-dissociation and the infrared OH-emission. Ann. Géophys., 24, 173-184.

_____,and A. C. Aikin, 1968: Variations of polar mesospheric oxygen and ozone during auroral events. Planet. Space Sci., 16, 371-384.

Mukherjee, B. K., and Bh. V. R. Murty, 1972: High level warmings over a tropical station. Mon. Wea. Rev., 100, 674-681.

Nicolet, M., 1971: Aeronomic reactions of hydrogen and ozone. Mesospheric Models and Related Experiments, G. Fiocco, ed., Dordrecht-Holland, D. Reidel Publ. Co., 1-51.

Noxon, J. F., 1964: The latitude dependence of OH rotational temperature in the night airglow. J. Geophys. Res., 69, 4087-4092.

Omholt, A., 1971: The Optical Aurora, New York, Springer-Verlag, 114-115.

Packer, D. M., 1961: Altitudes of the night airglow radiations. Ann. Géophys., 17, 67-75.

Potter, A. E., Jr., R. N. Coltharp, and S. D. Worley, 1971: Mean radiative lifetime of vibrationally excited (ν = 9) hydroxyl. Rate of the reaction of vibrationally excited hydroxyl (ν = 9) with ozone. J. Chem. Phys., 54, 992-996.

Poultney, S. K., 1974: Times, locations, and significance of cometary micrometeoroid influxes in the earth's atmosphere. Space Research XIV, Berlin, Akademie -Verlag, 707-708.

Quiroz, R. S. , 1970: Modification of the atmospheric density field in response to stratospheric warmings. Proc. Fourth Natl. Conf. Aerospace Meteorology, Las Vegas, Nev., Amer. Meteor. Soc., 296-305.

_____, 1971: The determination of the amplitude and altitude of stratospheric warmings from satellite-measured radiance changes. J. Appl. Meteor., 10 555-574

Reed, E. I., W. B. Fowler, and J. E. Blamont, 1973: An atlas of low-latitude 6300 A (OI) night airglow from Ogo-4 observations. J. Geophys. Res., 78, 5658-5675.

_____,and S. Chandra, Aug. 1974: The global characteristics of atmospheric emissions in the lower thermosphere and their aeronomic implications, GSFC X-621-74-246. Submitted to J. Geophys. Res.

Rogers, J. W., R. E. Murphy, A. T. Stair, Jr., and J. C. Ulwick, 1973: Rocket-borne radiometric measurements of OH in the auroral zone. J. Geophys. Res., 78, 7023-7031.

Rowe, J. N., A. J. Ferraro, H. S. Lee, and A. P. Mitra, 1969: Changes in electron density and collision frequency at University Park, Pennsylvania during, the stratospheric warming of 1967-68. J. Atmos. Terr. Phys., 31, 1077-1084.

Rundle, H. N., and H. M. Sullivan, 1972: Upper atmospheric sodium and stratospheric warmings. J. Atmos. Sci., 29, 977-981.

Shefov, N. N., 1972: Hydroxyl emission. Ann. Géophys., 28, 137-143.

Sivjee, G. G., K. A. Dick, and P. D. Feldman, 1972: Temporal variations in night-time hydroxyl rotational temperature. Planet. Space Sci., 20, 261-269.

Srivastava, A. N., and R. V. Shukla, 1970: Excitation mechanism of Na-D lines in the nightglow. Ann. Géophys., 26, 501-504.

Staff, Stratospheric Research Group, Free University Berlin, 1968: Daily and monthly Northern Hemisphere 5-millibar synoptic weather maps of the year October 1967-September 1968, Meteor. Abh. Berlin, Verlag von Dietrich Reimer.

Staff, Upper Branch, Nat. Meteor. Center, ESSA, 1970: Weekly synoptic analyses, 5-, 2-, and 0.4-millibar surfaces for 1967. ESSA Tech. Rept. WB 12, U. S. Government Printing Office, Wash., D. C., 169 pp.

_____, NOAA, 1971: Weekly synoptic analyses, 5- 2-, and 0.4-millibar surfaces for 1968. NOAA Tech. Rept. NWS 14, U. S. Government Printing Office, Wash., D. C., 169 pp.

Sullivan, H. M., 1971: Seasonal variation of the twilight sodium layer. J. Atmos. Terr. Phys., 33, 573-579.

Swider, W., Jr., 1969: Processes for meteoric elements in the E-region. Planet. Space Sci., 17, 1233-1246.

_____, 1970: Ionic reactions for meteoric elements. Ann. Geophys., 26, 595-599.

Tarasova, T. M. 1966: Night airglow in the region λ 6300 A. Cosmic Research, 4, 223-228.

U. S. Standard Atmosphere Supplements, 1966: Washington, D. C., U.S. Government Printing Office.

Visconti, G., and G. Fiocco, 1973: Increase of Na twilight emission after the Earth's crossing of the orbital planes of Comets Halley and Encke. J. Atmos. Terr. Phys., 35, 353-356.

Worley, S. D., R. N. Coltharp, and A. E. Potter, Jr., 1972: Rates of interaction of vibrationally excited hydroxyl (v = 9) with diatomic and small polyatomic molecules. J. Phys. Chem., 76, 1511-1514.

Figure Captions

Fig. 1 Synoptic maps for week of Jan 10, 1968 (Staff, NOAA, 1971). Note cold center near 75-80 N and 20 W.

Fig. 2 Temperature-time section of West Geirinish. (After Johnson, 1969). Temperatures are in degrees Celsius. Note the stratospheric warming near 45 km about Dec 21, the isothermal stratosphere about Dec. 31, the warm center at 65 km on Jan. 7-9, and the slight reestablishment of the stratopause after Jan. 7.

Fig. 3 Northern Hemisphere polar emission-rate maps for Jan. 7 Ogo-4 measured Na and OH nightglows. Emission rates are R A^{-1} for Na and R(100A)$^{-1}$ for OH. Blank areas indicate no available data. Orbit paths and orbit numbers indicated. Compare area of very high OH emission with synoptic maps of Fig. 1.

Fig. 4 Ogo-4 measured Na and OH emission rates in the region 0 W to 50 W and 60 N to 80 N in December 1967 and January 1968. Note that data is not available on some days. Emission rates correspond to kR A^{-1} for Na and kR (100A)$^{-1}$ for OH.

Fig. 5 Emission rates measured by Ogo-4 through filters centered at 3914, 5577, 5893 (Na), 6225 (OH), and 6300 A for Orbits 2365, 2394, and 2395 through area of 0 W to 50 W and 60 N to 80 N. Emission rates are kR A^{-1} for all but the 6225 A (OH) data, for which the emission rate is kR $(100A)^{-1}$.

Fig. 6 (a) Averaged Na and OH emission rates from data displayed in Fig. 4. Emission rates correspond to R A^{-1} for Na and $R(100A)^{-1}$ for OH.

(b) Temperatures near 25 W, 70 N. Daily temperatures for 5 mb (∿35 km) surface estimated from Staff (FUB, 1968). Weekly temperatures for 0.4 mb (∿51 km) surface estimated from Staff (Essa, 1970) and Staff (NOAA, 1971)

Figs. 7 and 8

(a) Model standard temperature profile and mesospheric warming layer.

(b) Percent deviations of temperature and density from standard mesosphere values due to mesospheric warming.

(c) Vertical profiles of the OH emission rate for the two temperature curves shown in (a).

(d) Vertical profiles of the Na emission rate for the two temperature curves shown in (a). Excitation mechanisms: "C" for Chapman scheme; "Ox" for O_2^* scheme; "B" for the two schemes of Bates and Nicolet.

(e) Percentage change in $[O_3]$ due to mesospheric warming shown in (a).

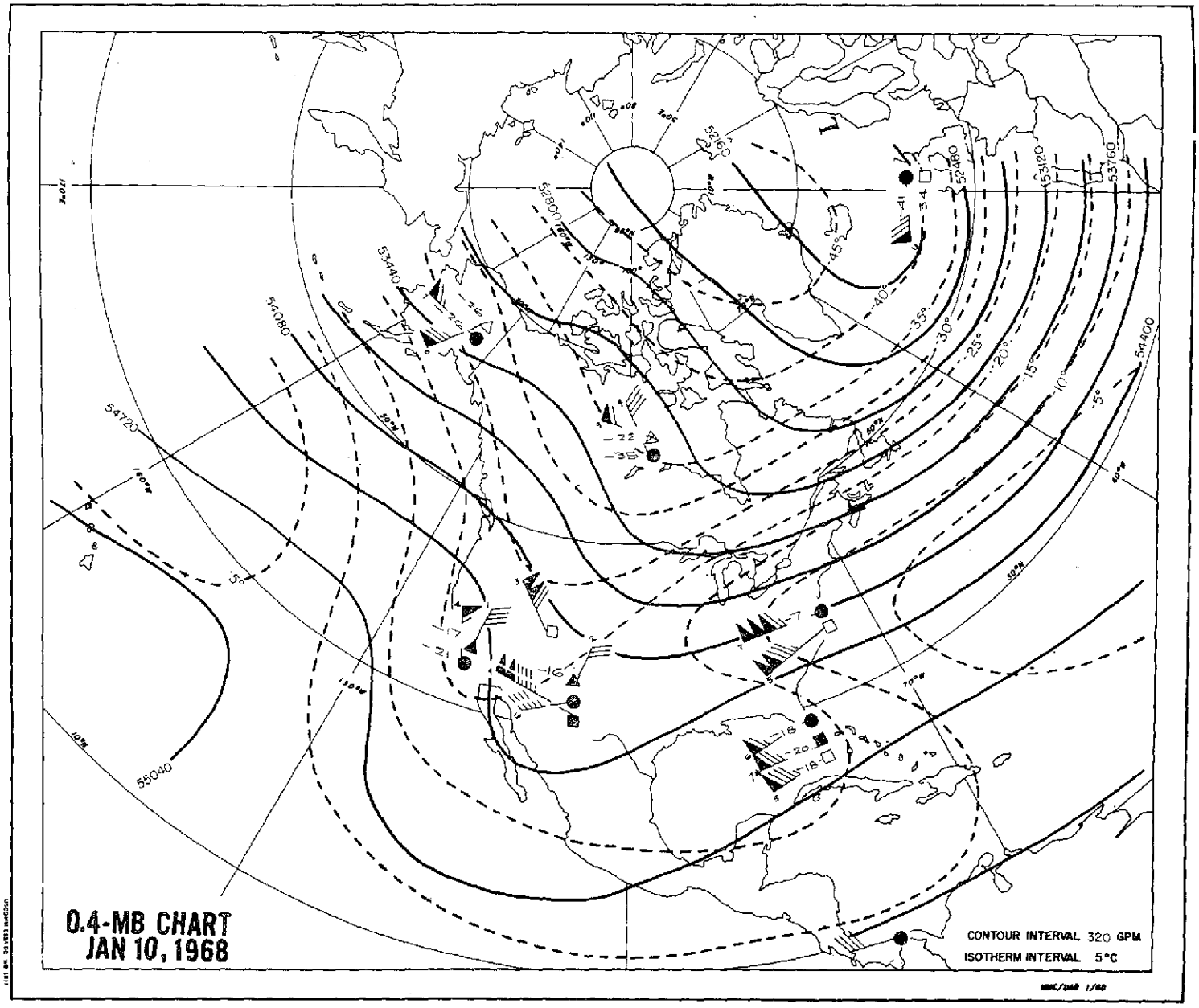
0.4-MB CHART
JAN 10, 1968
CONTOUR INTERVAL 320 GPM
ISOTHERM INTERVAL 5°C
L
53480
53120
53760
54400
54080
53440
54720
55040
-41
-34
-45°
-40°
-35°
-30°
-25°
-20°
-15°
-10°
-5°
-22
-35
-16
-21
-18
-20
-18
150°W
120°W
90°W
60°W
30°W
0°
30°N
50°N
70°N

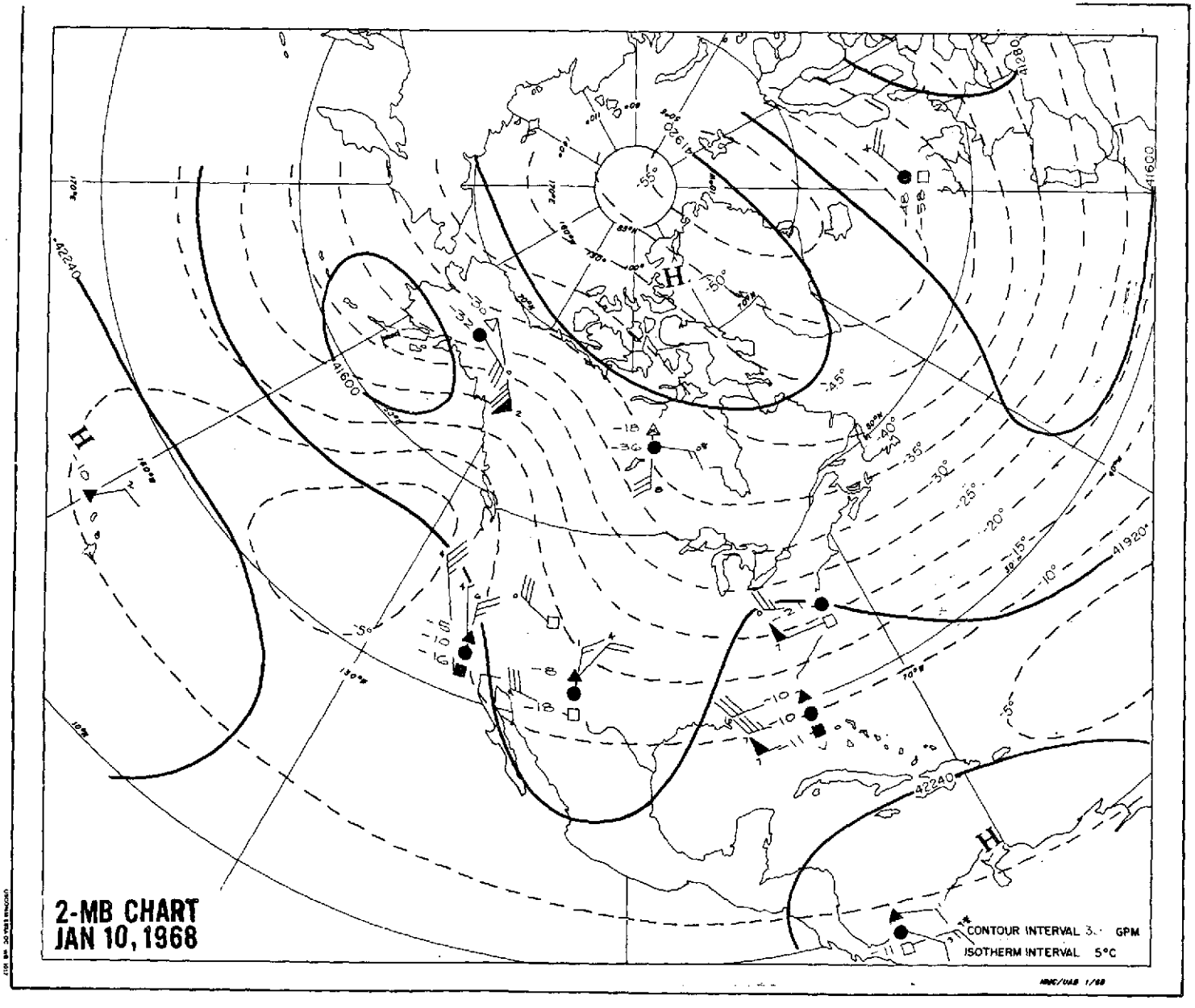
2-MB CHART
JAN 10, 1968
CONTOUR INTERVAL 3.. GPM
ISOTHERM INTERVAL 5°C
NMC/UAB 1/68

1b

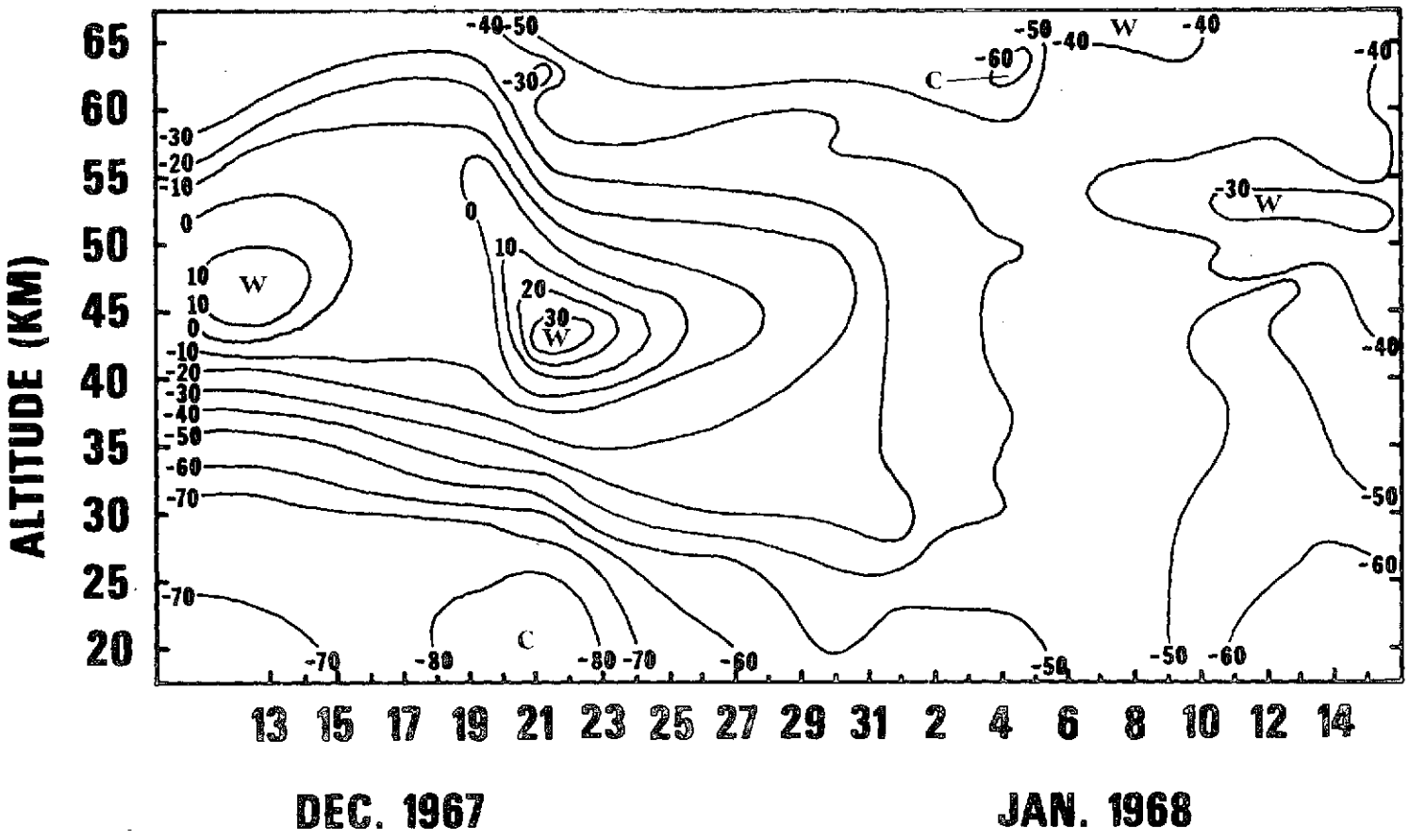
ALTITUDE (KM)
65
60
55
50
45
40
35
30
25
20
13 15 17 19 21 23 25 27 29 31 2 4 6 8 10 12 14
DEC. 1967
JAN. 1968
W
C

Fig. 2

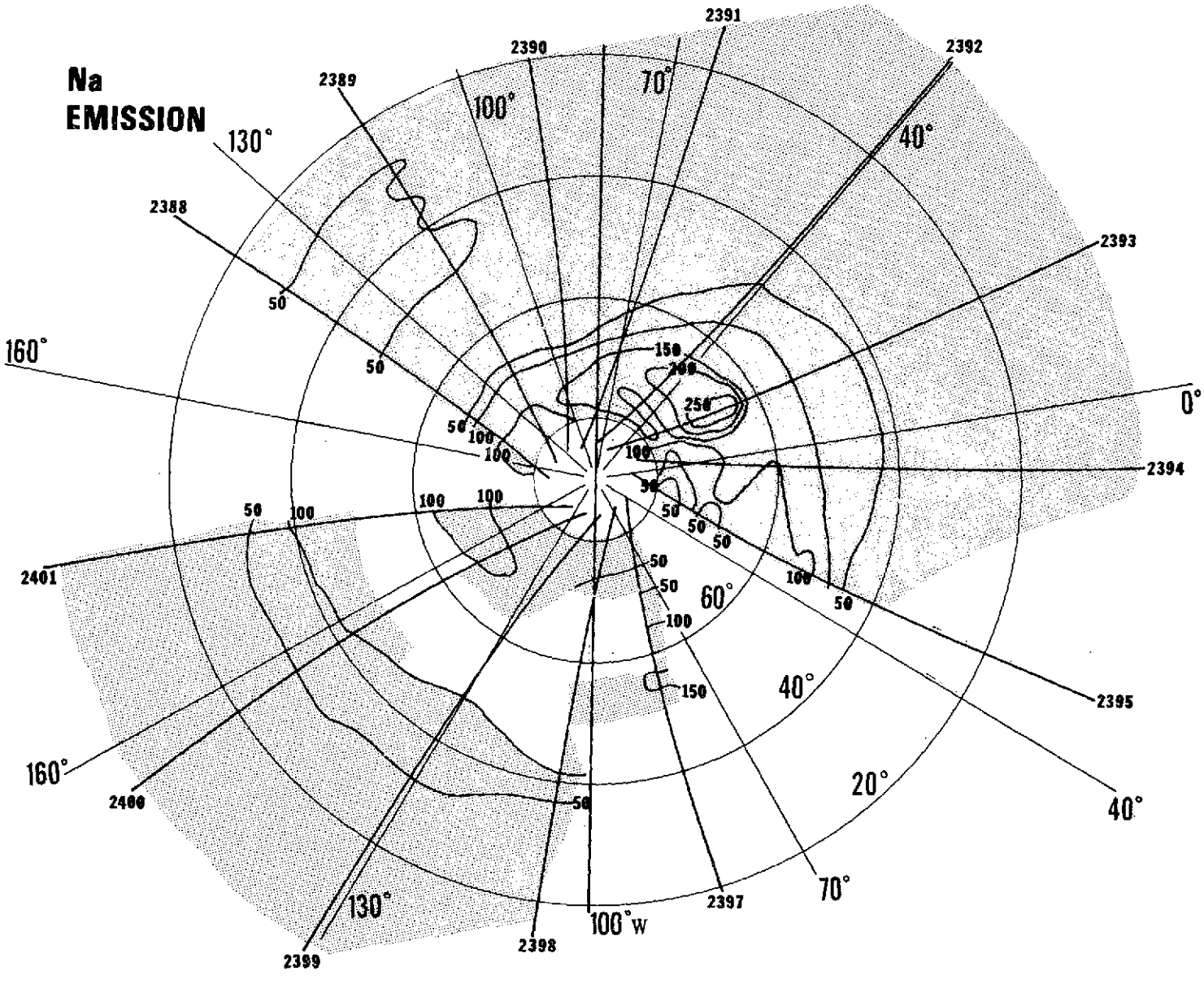
Na
EMISSION
2388
2389
2390
2391
2392
2393
2394
2395
2397
2398
2399
2400
2401
130°
100°
70°
40°
160°
0°
60°
20°
100°W
50
100
150
200
250

Fig. 3

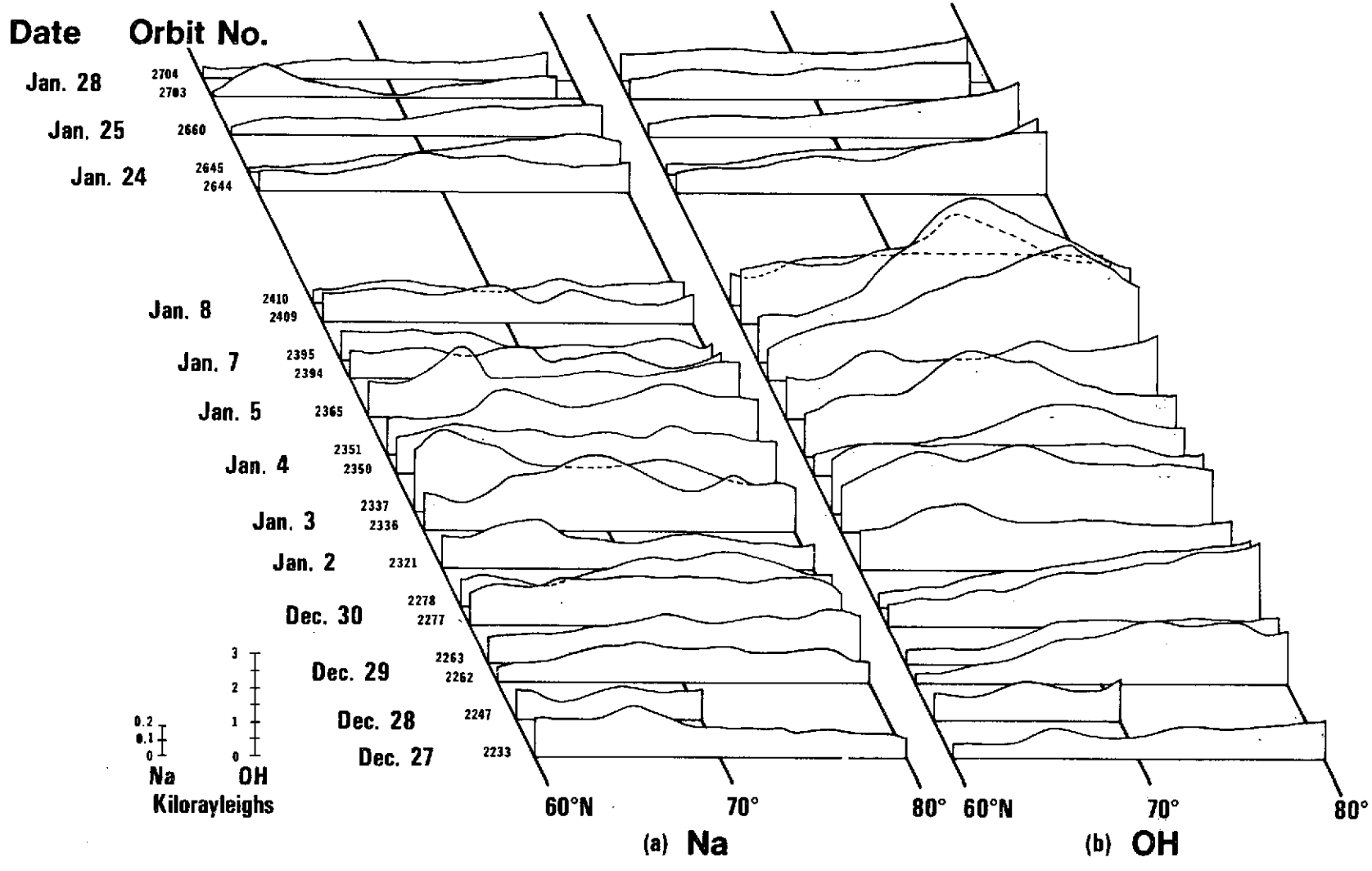
Date
Orbit No.
Jan. 28
2704
2703
Jan. 25
2660
Jan. 24
2645
2644
Jan. 8
2410
2409
Jan. 7
2395
2394
Jan. 5
2365
Jan. 4
2351
2350
Jan. 3
2337
2336
Jan. 2
2321
Dec. 30
2278
2277
Dec. 29
2263
2262
Dec. 28
2247
Dec. 27
2233
3
2
1
0
0.2
0.1
0
Na
OH
Kilorayleighs
60°N
70°
80°
(a) Na
60°N
70°
80°
(b) OH

Fig. 4

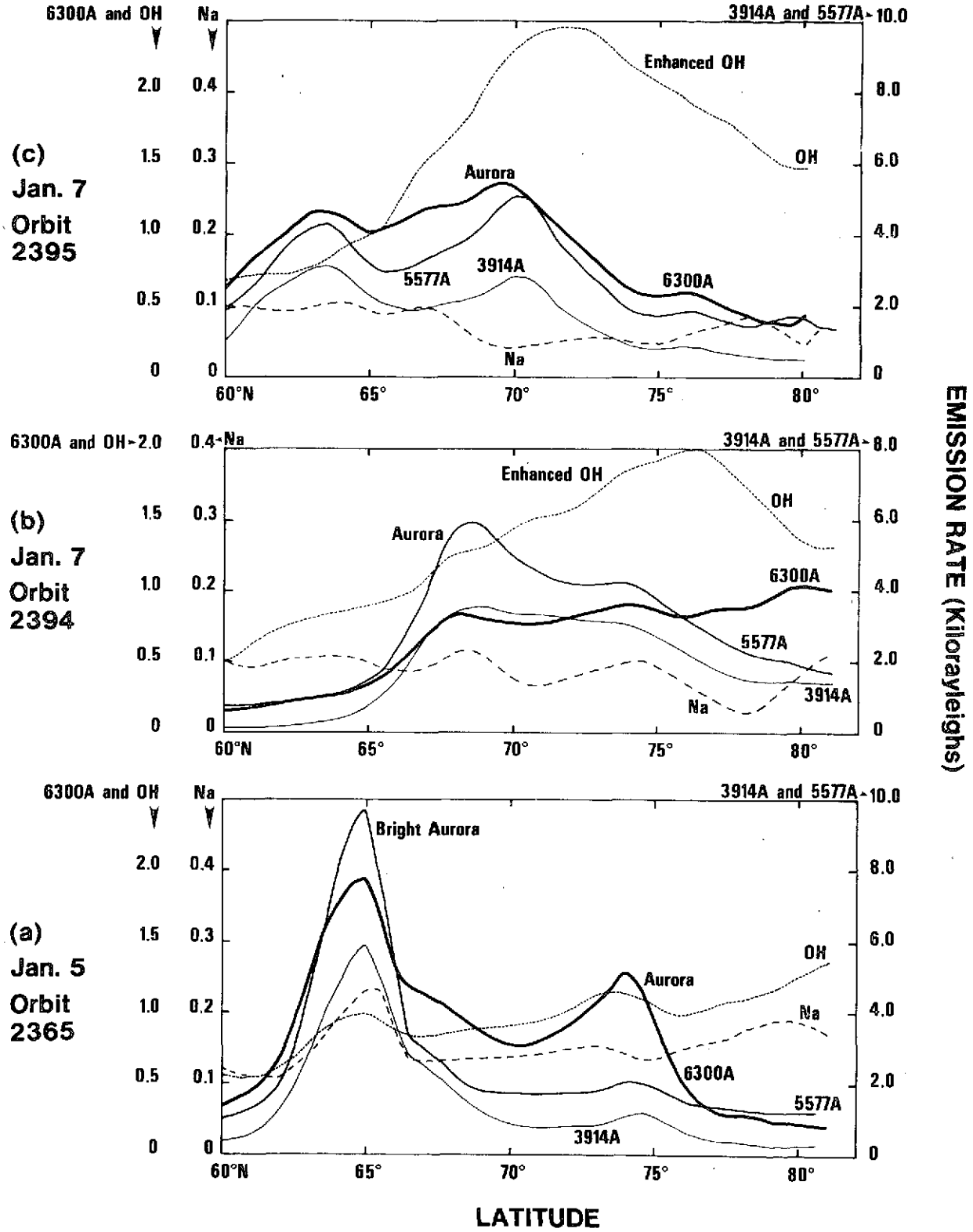
6300A and OH
Na
3914A and 5577A
(c)
Jan. 7
Orbit
2395
Enhanced OH
OH
Aurora
5577A
3914A
6300A
Na
60°N
65°
70°
75°
80°
(b)
Jan. 7
Orbit
2394
Enhanced OH
OH
Aurora
6300A
5577A
3914A
Na
(a)
Jan. 5
Orbit
2365
Bright Aurora
Aurora
OH
Na
6300A
5577A
3914A
LATITUDE
EMISSION RATE (Kilorayleighs)

Fig. 5

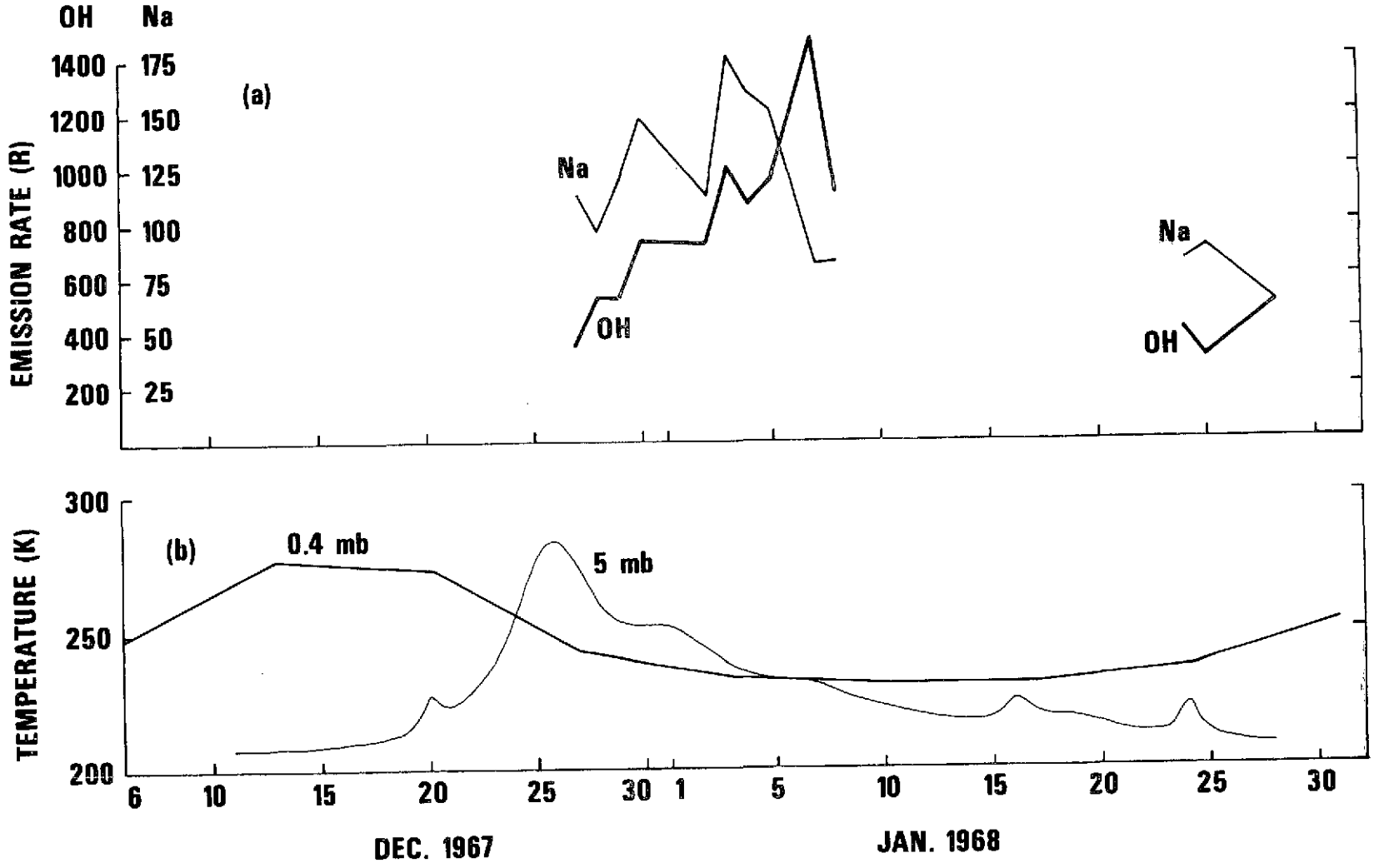
OH
Na
1400
1200
1000
800
600
400
200
175
150
125
100
75
50
25
(a)
EMISSION RATE (R)
Na
OH
Na
OH
300
250
200
TEMPERATURE (K)
(b)
0.4 mb
5 mb
6
10
15
20
25
30
1
5
10
15
20
25
30
DEC. 1967
JAN. 1968

Fig. 6

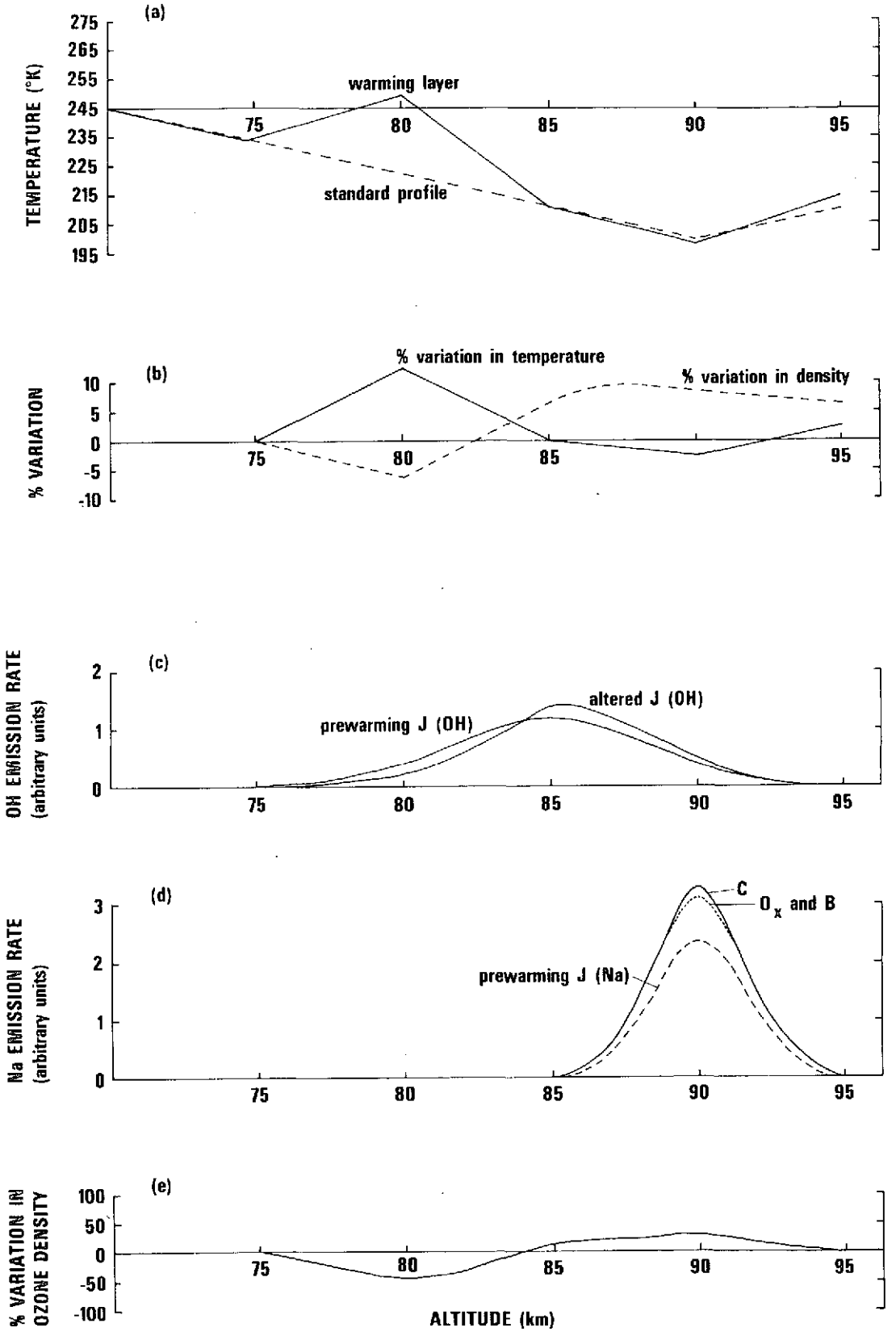
(a)
TEMPERATURE (°K)
275
265
255
245
235
225
215
205
195
warming layer
standard profile
75
80
85
90
95
(b)
% VARIATION
10
5
0
-5
-10
% variation in temperature
% variation in density
75
80
85
95
(c)
OH EMISSION RATE
(arbitrary units)
2
1
0
altered J (OH)
prewarming J (OH)
75
80
85
90
95
(d)
Na EMISSION RATE
(arbitrary units)
3
2
1
0
C
O_x and B
prewarming J (Na)
75
80
85
90
95
(e)
% VARIATION IN
OZONE DENSITY
100
50
0
-50
-100
75
80
85
90
95
ALTITUDE (km)

Fig. 7

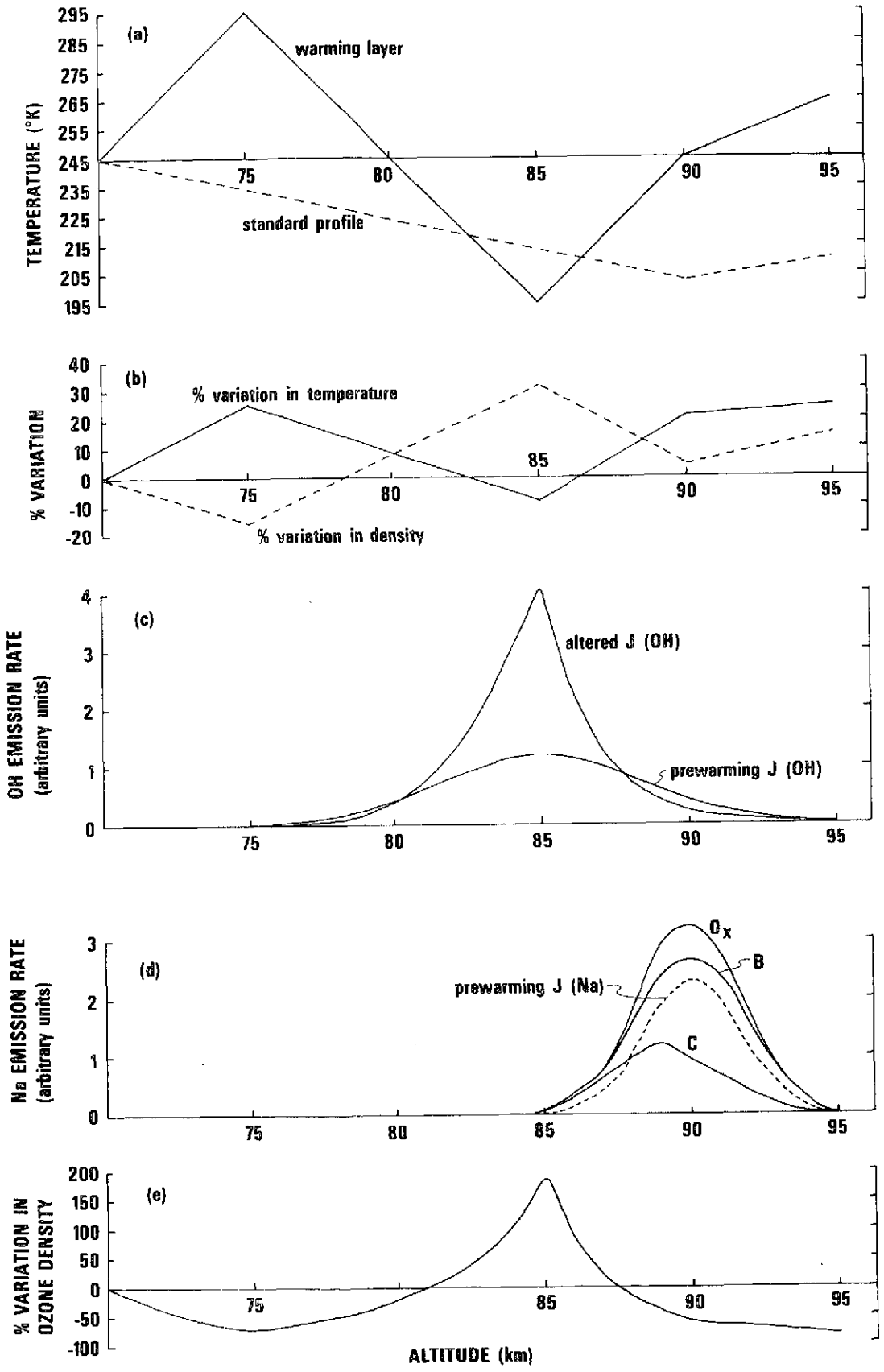
(a)
warming layer
standard profile
TEMPERATURE (°K)
295
285
275
265
255
245
235
225
215
205
195
75
80
85
90
95
(b)
% variation in temperature
% variation in density
% VARIATION
40
30
20
10
0
-10
-20
(c)
altered J (OH)
prewarming J (OH)
OH EMISSION RATE
(arbitrary units)
4
3
2
1
0
(d)
prewarming J (Na)
O_x
B
C
Na EMISSION RATE
(arbitrary units)
(e)
% VARIATION IN
OZONE DENSITY
200
150
100
50
0
-50
-100
ALTITUDE (km)

Fig. 8